

## Article

# Thermal Storage Performance of Underground Cave Dwellings under Kang Intermittent Heating: A Case Study of Northern China

Jiayin Zhu <sup>1</sup>, Yingfang Liu <sup>1</sup>, Ruixin Li <sup>1,\*</sup> , Bin Chen <sup>2</sup>, Yu Chen <sup>1</sup> and Jifu Lu <sup>1</sup>

<sup>1</sup> Department of Civil Engineering, Zhengzhou University, Zhengzhou 450001, China; zhujiayin1234@163.com (J.Z.); 17839940729@163.com (Y.L.); chenyu2021@zzu.edu.cn (Y.C.); jflu@zzu.edu.cn (J.L.)

<sup>2</sup> Laboratory of Building Environment and New Energy Resource, Dalian University of Technology, Dalian 116024, China; chenbin@dlut.edu.cn

\* Correspondence: andylrx@163.com; Tel.: +86-157-3670-2207

**Abstract:** The intermittent heating mode of Kang plays an important role in the heat storage and release in cave dwellings. However, research on the effect of Kang heating on the thermal process of traditional buildings is rare. Therefore, based on long-term monitoring of cave dwellings, regular conclusions about the influence of Kang heating on the thermal environment were obtained. Furthermore, an unsteady heat transfer model of the envelope was proposed for the first time. Then, based on this model, the thermal storage performance of cave dwellings during the period of Kang intermittent heating was explored. The results showed that, due to Kang heating, the indoor air temperature of cave dwellings could be increased by an average of 3.1 °C. Furthermore, the inner walls had a large thermal mass and the maximum heat storage in a single day was 487.75 kJ/m<sup>2</sup>, while the maximum heat release was 419.02 kJ/m<sup>2</sup>. The heat release at night could reach 87%. In this paper, the law of thermal storage and release characteristics of earthen building envelopes under intermittent heating was firstly obtained. Results can enrich the thermal process theory of earthen buildings and provide a theoretical basis and technical support for building thermal environmental construction.

**Keywords:** underground cave-dwelling; indoor thermal environment; thermal storage characteristics; Kang intermittent heating; unsteady heat transfer model



**Citation:** Zhu, J.; Liu, Y.; Li, R.; Chen, B.; Chen, Y.; Lu, J. Thermal Storage Performance of Underground Cave Dwellings under Kang Intermittent Heating: A Case Study of Northern China. *Processes* **2022**, *10*, 595. <https://doi.org/10.3390/pr10030595>

Academic Editor: Ambra Giovannelli

Received: 9 February 2022

Accepted: 16 March 2022

Published: 18 March 2022

**Publisher's Note:** MDPI stays neutral with regard to jurisdictional claims in published maps and institutional affiliations.



**Copyright:** © 2022 by the authors. Licensee MDPI, Basel, Switzerland. This article is an open access article distributed under the terms and conditions of the Creative Commons Attribution (CC BY) license (<https://creativecommons.org/licenses/by/4.0/>).

## 1. Introduction

With the background of global warming and carbon neutralization, it is necessary to excavate low-carbon and sustainable development strategies from traditional dwellings. Due to recyclability, low energy consumption, and low hidden carbon footprint, the traditional earthen buildings were considered as economically and environmentally sustainable buildings. A series of studies on earthen buildings has been carried out [1–5]. In China, there is a special earthen dwelling—the cave dwelling (nearly 90% of its structure built with earth), widely distributed in the cold Loess Plateau, which is the most extant form of ancient cave dwellings in the world [6]. Because of its good climate adaptability and low energy consumption, as of the end of the 20th century, more than 40 million people still lived in cave dwellings [7,8]. Therefore, increasing interest in cave dwellings has emerged in recent decades.

Current research on cave dwellings mainly has focused on two aspects. One is to obtain the thermal response of cave dwellings to outdoor climate through thermal environment monitoring. For example, in western Henan and Shanxi regions where the cave dwellings are densely distributed, a series of studies for different types of cave dwellings was conducted by Zhu's research group [8–11] and Liu's research group [6,12,13], and the thermal characteristics of local traditional cave dwellings were acquired. The results

showed that the fluctuations of the indoor thermal environment have been effectively suppressed by the heavy wall, and a stable indoor thermal environment was maintained. On the other hand, scholars focused on the thermal feelings of the residents in the cave dwellings, and a large number of studies on the thermal comfort of the cave dwellings was conducted. For example, based on Fanger's thermal comfort theory, the thermal comfort levels of cave rooms were evaluated by Li Xueping et al. [14,15]. The results indicated that the effects of ambient environment fluctuations on indoor conditions were effectively dampened to create a stable indoor thermal environment. Although there was still a small part of the time that failed to meet the existing standards, the study by Chengcheng Xu showed that traditional dwellers were more tolerant to harsh environments than the residents in urban regions. In addition, scholars found that earthen buildings present advantages in terms of thermal properties, due to their mass, thermal inertia, and moderated thermal conductivity. Furthermore, together with the high hygroscopicity of the earth, the indoor hygrothermal balance could be promoted [16,17].

It should be noted that unlike modern heating facilities relying on fossil fuels, the heating of cave dwellings uses biomass as fuel, including straw, stalks, wood and or other biomass, which are abundant in rural areas [18]. Biomass fuel has the advantages of renewable characteristics, but the disadvantages are also very obvious. In other words, a Kang often runs intermittently and cannot provide continuous and stable heat. However, previous research suggested that despite intermittent heating of the Kang, the indoor environment of the cave dwelling remained relatively stable [11]. This means that not only can the outdoor environment fluctuation be suppressed but also the influence of the fluctuation of the indoor heat source on the indoor thermal environment. An unsteady heat source needs heat storage equipment to maintain its stability [19]. Using the thermal mass of buildings' envelopes as thermal energy storage (TES) is a cost-effective solution [19]. Kang has a certain heat storage capacity. Scholars have conducted a series of studies where improvements of Kang on the thermal performance were carried out [20–24]. The recently improved Kang can reach a comprehensive heat efficiency between 70 and 80% [25]. However, the hourly heat dissipation of the Kang obtained by Xing Chaojie showed that the heat dissipation of the Kang still had large volatility, the Kang's combustion heating could only last for 2 h, and the heat storage capacity of the Kang itself was not enough to maintain the stability of the indoor thermal environment [11]. At present, many studies choose to use new materials, such as PCM [26–32] or CaO [33–36], as thermal storage materials, but additional investment costs are required by the new materials. The large thermal mass of the earthen envelope makes it the most suitable thermal storage equipment in cave dwellings. However, the research on the heat storage capacity of cave walls is still lacking.

The studies on the thermal characteristics of the earthen building envelope showed that the envelope of earthen buildings was usually thick, with large thermal mass and thermal inertia, which made the wall have good attenuation and delay characteristics [13,37]. Thus, the indoor air temperature was less influenced by the outdoor temperature, maintaining thermal stability. Therefore, the thermal performance calculation of the cave envelope is particularly important. Generally, there are two approaches, namely, the analytical method based on integral transformation and the numerical method based on finite difference or finite element [38–42]. For example, the recommended insulation thickness values to achieve heat preservation in the winter and heat insulation in the summer were given by Meng Chen [43], and the damping ratio of different thicknesses was obtained by Liu [12].

The above literature presenting most of the research on traditional cave dwellings has focused on the measurement and evaluation of thermal environments to excavate the thermal response of cave dwellings to outdoor climates. However, the response of wall heat storage characteristics to indoor heat source fluctuation is still lacking. To address the research gaps, a typical underground cave dwelling in the Yuxi area of northern China was used, for which the thermal environment parameters were monitored during the period of Kang intermittent heating. Furthermore, a calculation model for the unsteady heat transfer of the heavy wall was established based on the harmonic response method. The

quantitative data on the thermal storage performance of the wall of the caves was obtained. The novelty and scientific significance of this paper are to focus on the response of cave walls to indoor heat sources, the law of thermal storage, and release of the heavy wall under intermittent heating by biomass heating, which was revealed through quantitative data, providing a reference for exploring using the thermal mass of building envelopes as thermal energy storage.

## 2. Materials and Methods

### 2.1. Selection of the Case Studies

#### 2.1.1. Analyzed Settlement: Miaoshang Village

The loess of western Henan is usually alluvial loess. The soil is compact and boasts characteristics that include earthquake resistance, compression resistance, and convenience for vertical excavation construction, providing favorable soil conditions for the construction of cave dwellings, as shown in Figure 1. Considering the influence of the surrounding landforms and historical development, underground cave dwellings gradually became the main form of housing in Shan County of Sanmenxia city. The underground cave dwellings in Shan County have a long history of several hundred years. There are nearly 100 underground cave-dwelling villages, and each village has a relatively concentrated distribution of underground cave dwellings. In March 2013, Miaoshang Village was recognized by the State Council, adding to the seventh group of National Crucial Cultural Relics Protection Units. Therefore, under this condition of protection and renewal, the study of sunken courtyards and the dynamics of their protection in modern society would have broad significance. The underground cave dwellings with hundreds of years of existence in Miaoshang village, Shan County were selected for this study in which the thermal and humid environments in cold climate conditions were field-measured.



**Figure 1.** The distribution diagram of cave dwellings in western Henan.

#### 2.1.2. Geographical Position and Climate Features

Sanmenxia city is in the western Henan province along the shore of the Yellow River. Considering the influence of the larger tributaries of the Yellow River (Qinglong River and Canglong River), this area contains various topographies and geomorphologies, mainly in the mountains, loess hills, and loess tablelands. The villages are primarily concentrated in the loess tableland, and most of the dwellings are earthen cave dwellings.

Sanmenxia, a city with four distinctive seasons, is hot and rainy in the summer while cold and dry in the winter and belongs to the cold climate regions of China (Figure 2). The annual temperature and humidity distribution are shown in Figure 3a. The hottest month is July with an average temperature of 24.8 °C and average relative humidity of 81%. The

coldest month is January with an average temperature of  $-1.0\text{ }^{\circ}\text{C}$  and average relative humidity of 62%. In recent decades, the annual rainfall has decreased and continues to show a decreasing trend. As shown in Figure 3b, the rainfall in the summer is relatively concentrated, accounting for 47.4% of the total rainfall in the whole year, whereas rainfall in the winter is infrequent, accounting for only 3.2% of the total rainfall. The frost-free period lasts 215 days, the annual duration of sunshine is approximately 2261.7 h, and the total annual solar radiation is  $5274\text{ MJ/m}^2$ , ranking this city as a Class III city for solar energy resources.

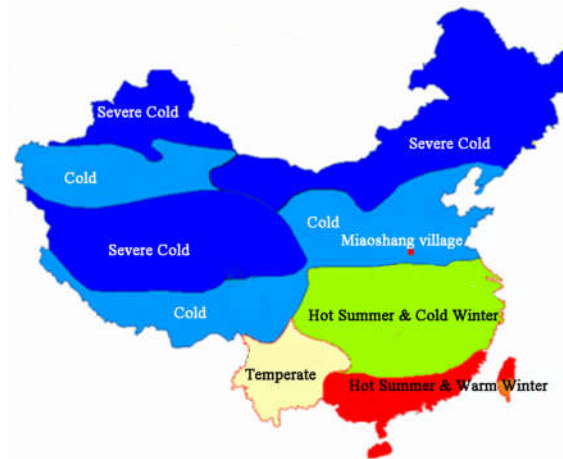


Figure 2. The map of the climate regions of China illustrates the site.

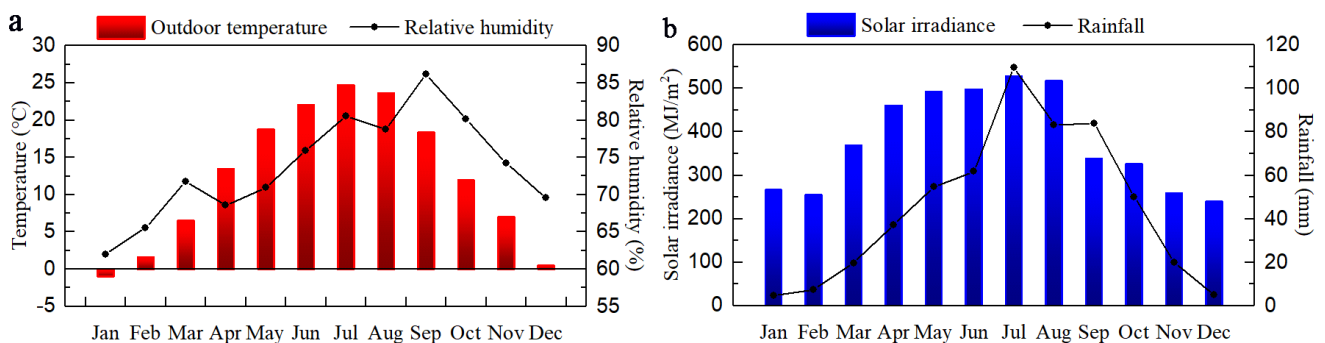


Figure 3. Climate data of Sanmenxia city: (a) annual temperature and humidity; (b) annual solar irradiance and rainfall.

### 2.1.3. Building Description: Analyzed Underground Cave Dwellings

The underground cave dwellings were often constructed using local construction techniques. A diagram of an underground cave room structure is shown in Figure 4. The closed courtyard was excavated vertically from the ground at a depth of approximately 5–8 m and the plane dimension can be up to  $15\text{ m} \times 15\text{ m}$ . Next, the soil walls around the courtyard were horizontally excavated to form the cave rooms. A ramp was built in one of these cave rooms (Figure 5a) as the entrance connecting to the ground level. The water ripples and saw-tooth patterns were etched only on the facade, as shown in Figure 5b, or on affixing bricks to prevent the scouring of rain and wind, enhancing the stability of the cave dwelling and ensuring the safety of the residents. The wall around the top of the facade acts as a parapet and prevents people and livestock from falling into the yard in addition to blocking the rain. The roof of the parapet is a shield that guides the flow of rainwater and protects the facade from scouring. There was a Kang installed in the back of the cave rooms monitored in this study. The chimney is located close to the wall and reaches ground level through the soil cover layer. The hood at the top of the chimney protects it from the wind and rain. A water well and dry well are located in the courtyard for water storage

and drainage. Fruit trees were often planted in the courtyard, which not only aesthetically enhanced the environment but also provided wind and rain protection as well as shade, creating a favorable micro-environment (Figure 5c).

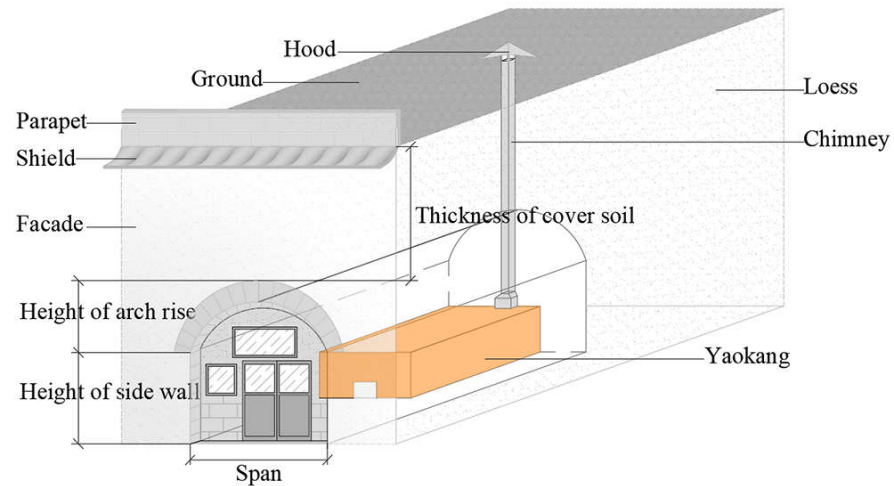


Figure 4. Structure diagram of the underground cave room.



Figure 5. Appearance of underground cave dwellings: (a) ramp; (b) facade; (c) courtyard.

Two underground cave dwellings with the same orientation (east-facing) and the same architectural structure in Miaoshang village, Shan County, Sanmenxia city were selected for monitoring. One of these dwellings is equipped with a Kang (located as shown in Figure 6a; this dwelling is abbreviated as “KCD”). The Kang-body is connected to the west internal wall and the south-facing wall. The chimney is close to the west internal wall. The other dwelling is without a Kang (abbreviated as “NKCD”). The interior and outdoor environments are shown in Figure 6b,c, respectively. Wooden single-glazed double doors and two non-openable single-glazed wooden windows are located on the external wall. The thermal properties of the envelopes and other pertinent building information are listed in Tables 1 and 2, respectively.



Figure 6. Photos of the selected underground cave dwelling: (a) Kang; (b) courtyard; (c) cave room.

**Table 1.** Thermal properties of envelopes.

Layers	Thickness (mm)	Density (kg/m <sup>3</sup> )	Conductivity (W/m·K)	Specific Heat (kJ/kg·K)	Heat Storage Coefficient (W/m <sup>2</sup> ·K)	Thermal Inertia
External wall						
Plaster	20	1800	0.93	0.84	10.11	6.63
Loess	260	1821	1.41	1.84	13.49	
Brick	60	1668	0.43	750	6.25	
West internal wall						
Plaster	20	1800	0.93	0.84	10.11	65.50
Loess	4500	1850	1.41	1.84	13.49	
South side wall						
Plaster	20	1800	0.93	0.84	10.11	21.99
Loess	1500	1850	1.41	1.84	13.49	
North side wall						
Plaster	20	1800	0.93	0.84	10.11	28.95
Loess	1980	1850	1.41	1.84	13.49	
Windows						
Single-layer glass	3	2500	0.76	0.84	10.69	
Door						
Wood	50	500	0.14	2.51	3.85	

**Table 2.** Building information of two cave rooms with same orientation.

Cave Names	Span (mm)	Depth (mm)	Height of Arch Rise (mm)	Height of Side Wall (mm)	Thickness of Cover Soil (mm)	Thickness of External Wall (mm)	Shape Coefficient	Window Wall Ratio
NKCD	3000	8400	1200	1800	4500	340	8.4	0.28
KCD	3200	7600	1200	1800	4500	340	7.6	0.28

## 2.2. On-Site Measurement

In this study, the on-site measurement was carried out in the coldest time of the year. The winter of Miaoshang village lasts from December to March, and normally the coldest period occurs in January. Hence, this research was conducted from 23 to 28 January 2019.

During the monitoring period, all the doors and windows of the cave rooms, which were uninhabited, were kept closed except when it was necessary to enter the room to add wood to burn in the Kang and record data. The mode of burning in the Kang followed local custom, as shown in Table 3. Indoor and outdoor air temperature and humidity, surface temperature, and air velocity were measured. Meanwhile, outdoor air temperature and humidity, air velocity, and illuminance were measured. All the measuring instruments were listed in Table 4, and the data were recorded at 10 min intervals.

**Table 3.** The way of burning Kang.

Date	23 January	24 January	25 January	26 January	27 January	28 January
Way of burning	Adding wood Burning at 9:00–10:00	Adding wood Smoldering	Adding wood Smoldering	No adding	No adding	No adding

The measurement points in the NKCD and KCD were arranged similarly to ensure the comparability of the test results. Five points from the door to the back of the room and three points at different heights of the room along the height were evenly distributed according to the Standard for Energy Efficiency Test of Residential Buildings [44]. The parameters of the outdoor thermal environment were measured with points located on a

tree in the courtyard 1.5 m from the courtyard ground. Details regarding the arrangement are shown in Figure 7.

**Table 4.** Monitored data and technical specifications of measuring instruments.

Monitoring Parameters	Instrument Name	Measurement Range	Accuracy	Resolution
Air temperature and relative humidity	Fluke 971	temperature: −20~60 °C relative humidity: 5~95%	temperature: ±0.5 °C (0~45 °C) ±1.0 °C (−20~0 °C, 45~60 °C) relative humidity: ±5% (<10%, >90%) ±1.5 °C (10~90%)	temperature: 0.1 °C relative humidity: 0.1%
Surface temperature	Testo 830-S1	−30~350 °C		0.1 °C
Wind velocity	Testo 405-V1	0~10 m/s	±0.1 m/s ± 5% reading (<2 m/s) ±0.3 m/s ± 5% reading (>2 m/s) ± 3% rdg ± 5% f.s. (<10,000 Lux); ± 4% rdg ± 10% dgts. (>10,000 Lux);	0.01 m/s
Illuminance	HT-1318	0~400 k Lux		1 Lux

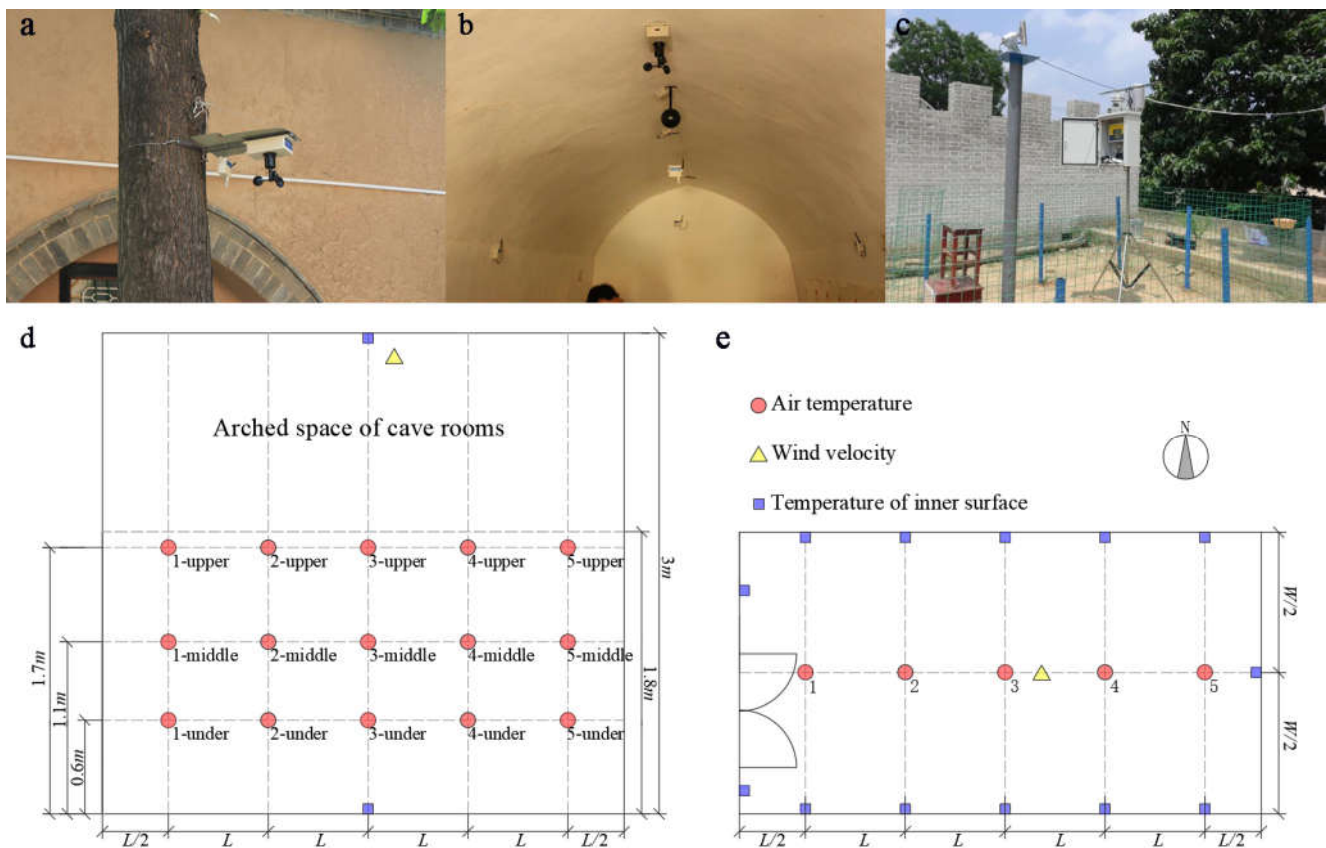


**Figure 7.** Arrangement layout of points of photo: (a) indoor; (b) courtyard; (c) ground; (d) profile of indoor points; (e) planar graph of indoor points.

### 2.3. Theoretical Calculation

#### 2.3.1. Fourier Series Expansion of Double-Sided Thermal Effect

A comprehensive outdoor temperature expresses the thermal effect of the outdoor air temperature, solar radiation, ground reflection radiation, longwave radiation, and atmospheric longwave radiation on the external surface of the wall. Therefore, it is more accurate to analyze the heat transfer of the external walls using this comprehensive outdoor temper-

ature as the outdoor thermal effect. According to References [45,46], the comprehensive outdoor temperature can be calculated using Equation (1).

$$t_z = t_a + \frac{q_U + q_R}{\alpha_a} - \frac{q_e}{\alpha_a} \quad (1)$$

where  $t_a$  is the outdoor dry-bulb temperature in °C,  $q_U$  is the solar radiation in W/m<sup>2</sup>,  $q_R$  is the ground reflection in W/m<sup>2</sup>,  $\alpha_a$  is the total surface heat transfer coefficient of the external wall in W/m<sup>2</sup>·K, and  $q_e$  is the nocturnal radiation in W/m<sup>2</sup>.

To ensure the fitting accuracy of the comprehensive outdoor temperature, the discrete comprehensive outdoor temperature was expanded using the Fourier series with the combination of six multi-harmonic solutions with  $\pi/12$  as the fundamental frequency.

The Fourier series expansion of comprehensive outdoor temperature is

$$\begin{aligned} t_{z,f} = & 3.26 + 6.77 \sin\left(\frac{\pi}{12}\tau + 4.20\right) + 2.30 \sin\left(\frac{\pi}{6}\tau + 1.64\right) \\ & + 0.05 \sin\left(\frac{\pi}{4}\tau + 2.54\right) + 0.71 \sin\left(\frac{\pi}{3}\tau + 4.55\right) \\ & + 0.32 \sin\left(\frac{\pi}{2}\tau + 0.59\right) + 0.52 \sin\left(\frac{7\pi}{12}\tau + 2.79\right) \end{aligned} \quad (2)$$

The Fourier series expansion of indoor temperature in NKCD is

$$\begin{aligned} t_{nr,f} = & 6.97 + 0.91 \sin\left(\frac{\pi}{12}\tau + 3.59\right) + 0.22 \sin\left(\frac{\pi}{6}\tau + 0.28\right) \\ & + 0.16 \sin\left(\frac{\pi}{4}\tau + 1.49\right) + 0.11 \sin\left(\frac{\pi}{3}\tau + 4.43\right) \\ & + 0.05 \sin\left(\frac{\pi}{2}\tau + 5.14\right) + 0.05 \sin\left(\frac{7\pi}{12}\tau + 0.4\right) \end{aligned} \quad (3)$$

The Fourier series expansion of indoor temperature in KCD is

$$\begin{aligned} t_{kr,f} = & 7.86 + 1.78 \sin\left(\frac{\pi}{12}\tau + 3.78\right) + 0.68 \sin\left(\frac{\pi}{6}\tau + 1.87\right) \\ & + 0.20 \sin\left(\frac{\pi}{4}\tau + 1.99\right) + 0.11 \sin\left(\frac{\pi}{3}\tau + 5.40\right) \\ & + 0.20 \sin\left(\frac{\pi}{2}\tau + 5.14\right) + 0.18 \sin\left(\frac{7\pi}{12}\tau + 1.70\right) \end{aligned} \quad (4)$$

According to Equations (2)–(4), Fourier fitting curves were obtained, as shown in Figure 8.

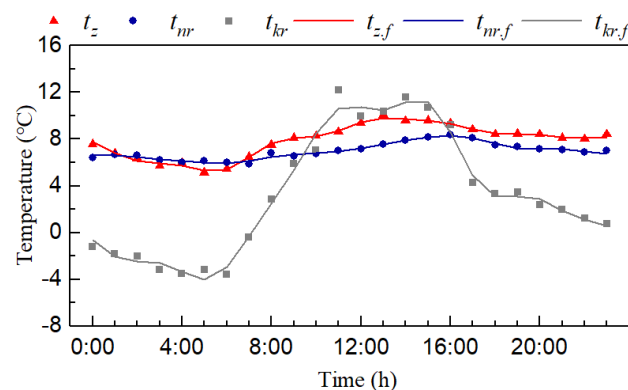


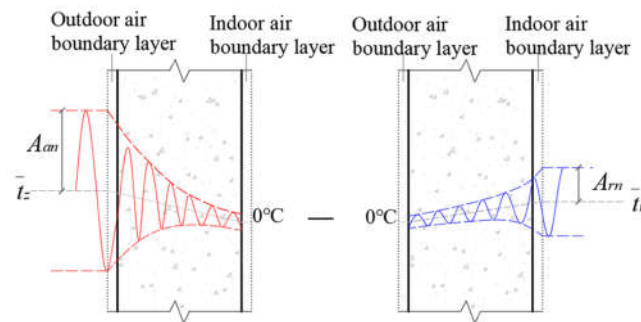
Figure 8. Fitting curves of indoor and outdoor temperature.

Figure 8 shows that the fitting curves expanded using Fourier series in six multi-harmonic solutions coincides with the discrete value very well. This indicates that the functions of the Fourier series expansion can accurately represent the fluctuations in the indoor and outdoor thermal effects.

### 2.3.2. Heat Transfer of the Heavy Wall under Double-Sided Thermal Effect

Based on the thermal inertia of the wall, the indoor and outdoor temperature waves are attenuated and delayed during the thermal transfer through the external wall. Therefore,

the heat flux of the external wall can be considered as the difference between the following two conditions, as shown in Figure 9.



**Figure 9.** Attenuation of the thermal waves.

(1) When the indoor air temperature  $t_r = 0$ , the comprehensive outdoor temperature is attenuated and delayed. The unsteady heat transfer from the outside to the inside is

$$q_1(\tau) = k \left[ -\frac{\alpha_r}{k} \sum_{n=1}^{N/2} \frac{A_{an}}{v_{yn}} \sin(\omega_n \tau + \varphi_{an} - \psi_{yn}) - \bar{t}_z \right] \quad (5)$$

where  $k$  is heat transfer coefficient of the wall in  $\text{W}/(\text{m}^2 \cdot \text{K})$ ;  $\alpha_r$  is convective heat transfer coefficient in  $\text{W}/(\text{m}^2 \cdot \text{K})$ ;  $n$  is an order of harmonic  $1, 2 \dots 6$ ;  $N$  is the number of discrete points in the period with value of 24;  $A_{an}$  is the amplitude of each harmonic of outdoor thermal waves;  $\varphi_{an}$  is the initial phase of each harmonic of outdoor thermal waves;  $\omega$  is the harmonic frequency of each;  $v_{yn}$  is attenuation multiple of sine temperature wave with different frequencies on the outdoor of the wall determined by Equation (6);  $\psi_{yn}$  is delay phase of sine temperature wave with different frequencies on the outdoor of the wall; and  $v_{yn}$  and  $\xi_{yn}$  are the thermal frequency response of heat transfer of wall.

$$v_{yn} = \alpha_r |B(i\omega n)| = \alpha_r \sqrt{B(i\omega n)_{Res}^2 + B(i\omega n)_{Im}^2} \quad (6)$$

$$\psi_{yn} = \frac{2\pi}{T} \xi_{yn} = \arctan \left[ \frac{B(i\omega n)_{Im}}{B(i\omega n)_{Res}} \right] \quad (7)$$

where  $\xi_{yn}$  is the delay time of sine temperature wave with different frequencies on the outdoor of the wall,  $B(i\omega n)_{Res}$  and  $B(i\omega n)_{Im}$  are the real and imaginary parts of the  $B$  element in the wall Heat Transfer Matrix (the solving method of Heat Transfer Matrix is shown in References [45,46]), and  $T$  is cycled with a value of 24.

(2) When the outdoor air temperature  $t_z = 0$ , the comprehensive indoor temperature is attenuated and delayed. The unsteady heat transfer from the inside to the outside is

$$q_2(\tau) = k \left\{ \frac{\alpha_r}{k} \sum_{n=1}^{N/2} A_{rn} \left[ \frac{1}{v_{zn}} \sin(\omega_n \tau + \varphi_{rn} - \psi_{zn}) - \sin(\omega_n \tau + \varphi_{rn}) \right] - \bar{t}_r \right\} \quad (8)$$

where  $v_{zn}$  is attenuation multiple of sine temperature wave with different frequencies on the indoor of the wall determined by Equation (9),  $\varphi_{rn}$  is the initial phase of each harmonic of indoor thermal waves,  $\psi_{zn}$  is delay phase of sine temperature wave with different frequencies on the indoor of the wall, and  $v_{zn}$  and  $\psi_{zn}$  are the thermal frequency response of heat transfer of wall.

$$v_{zn} = \frac{|B(i\omega_n)|}{|B_0(i\omega_n)|} \quad (9)$$

$$\psi_{zn} = \frac{2\pi}{T} \xi_{zn} = \arctan \left[ \frac{B(i\omega_n)}{B_0(i\omega_n)} \right] \quad (10)$$

where  $\xi_{zn}$  is the delay time of the sine temperature wave with different frequencies at the internal side of the wall.

The heat flux through the wall  $q$  is obtained by the following equation.

$$q(\tau) = q_1(\tau) - q_2(\tau) = k(\bar{t}_r - \bar{t}_z) - \alpha_r \sum_{n=1}^{N/2} \frac{A_{an}}{v_{yn}} \sin(\omega_n \tau + \varphi_{an} - \psi_{yn}) - \alpha_r \sum_{n=1}^{N/2} A_{rn} \left[ \frac{1}{v_{zn}} \sin(\omega_n \tau + \varphi_{rn} - \psi_{zn}) - \sin(\omega_n \tau + \varphi_{rn}) \right] \quad (11)$$

According to Equation (11), under the effects of periodic thermal effect, the unsteady heat transfer through the external wall can be a result of three aspects (Figure 10):

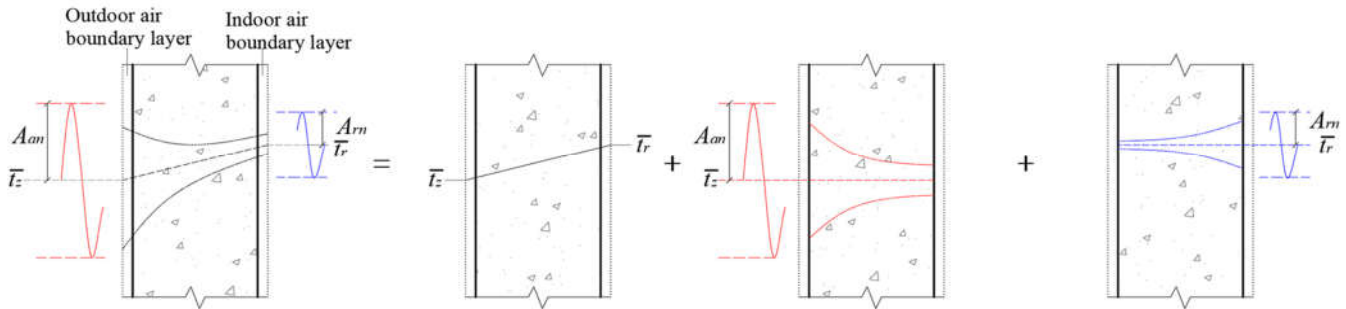


Figure 10. Schematic diagram of heat transfer calculation.

The steady heat transfer is caused by the difference between the average comprehensive outdoor temperature and the average indoor air temperature,

$$q_s = k(\bar{t}_r - \bar{t}_z) \quad (12)$$

the additional heat transfer due to the effect in the comprehensive outdoor temperature fluctuation,

$$q_a = -\alpha_r \sum_{n=1}^{N/2} \frac{A_{an}}{v_{yn}} \sin(\omega_n \tau + \varphi_{an} - \psi_{yn}) \quad (13)$$

and the additional heat transfer due to effect in the indoor air temperature fluctuation,

$$q_r = -\alpha_r \sum_{n=1}^{N/2} A_{rn} \left[ \frac{1}{v_{zn}} \sin(\omega_n \tau + \varphi_{rn} - \psi_{zn}) - \sin(\omega_n \tau + \varphi_{rn}) \right] \quad (14)$$

### 2.3.3. Unsteady Heat Transfer Model Validation

To analyze and verify the model, heat flux data of the external wall collected on 23 January were selected for comparison. The differences between the simulated and measured data during this period are presented in Figure 11.

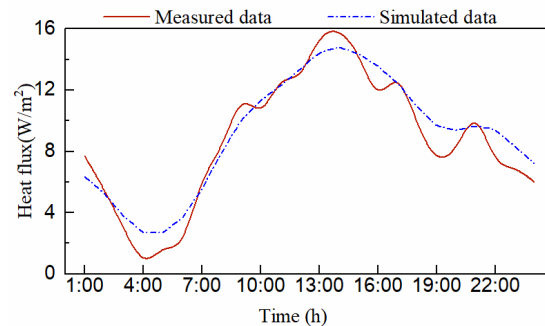


Figure 11. The agreement between the simulation and the monitoring results.

The normalized mean bias error (NMBE) and the coefficient of variation (CV) of the root mean square bias error (RMSE) were used to evaluate the consistency of the normalized

mean bias error (NMBE). The NMBE value indicates the existence of systematic error or deviation, while CV (RMSE) is a powerful indicator of simulation accuracy [47]. NMBE and CV (RMSE) are defined as follows:

$$\text{NMBE}(\%) = \frac{\sum_{i=1}^n (t_{ip} - t_{im})}{n - 1} \times \frac{1}{t_m} \times 100 \quad (15)$$

$$\text{CV}(\text{RESM})(\%) = \sqrt{\frac{\sum_{i=1}^n (t_{ip} - t_{im})^2}{n - 1}} \times \frac{1}{t_m} \times 100 \quad (16)$$

where  $t_{ip}$  is the simulated temperature of node  $i$ ,  $t_{im}$  is the monitored temperature of node  $i$ ,  $t_m$  is the arithmetic mean of a sample of  $n$  measured data, and  $n$  is the number of monitored data points (temperatures) during the monitoring period.

The NMBE value of 5.22% and the CV (RMSE) value of 17.35% were far below the requisite specified maximum of 25% [47]. Hence, the NMBE and CV (RMSE) parameters verified the validity of the model for calculating the heat flux of the wall, based on the mathematical model, and the thermal characteristics of the Kang can be further optimized. Based on the unsteady heat transfer model, the thermal performance of the external wall can be further analyzed.

The traditional unsteady heat transfer model usually only considers the influence of the fluctuation of the outdoor thermal disturbance, while the indoor and outdoor double-sided thermal effect were considered in the unsteady heat transfer model established in this paper. At the same time, the influence of the double-sided thermal effect on the heat transfer of the wall was split, which makes the relationship between the heat transfer and the thermal effect of the wall clearer and provides a theoretical basis for the heat transfer and storage analysis of the heavy wall.

### 3. Results and Discussion

#### 3.1. Thermal Performance of Cave Rooms under the Biomass Heating

The heavy envelope acts as an important heat storage mass for the cave rooms due to the advantage of having a slow heat storage-release rate. Part of the heat from the Kang is directly transmitted to the indoor air to increase the indoor air temperature through convection between the Kang-body and indoor air. The rest of the heat is stored in the wall through thermal radiation and conduction and is gradually released into the room through convection between the wall and air when the indoor temperature drops. Because these walls play an important role in maintaining a stable indoor temperature, the thermal performance of the cave rooms heated by this heat charging and discharging of the heavy walls was analyzed based on the measured data.

##### 3.1.1. Thermal Environment of the Underground Cave Dwellings

In this study, the temperature and relative humidity in the NKCD and KCD were quantitatively analyzed to verify the effectiveness of Kang heating, as shown in Figures 12 and 13, respectively.

Figure 12 shows that the outdoor temperature varied by 15.9 °C (from −6.8 °C to 9.1 °C) during the monitoring period, whereas the indoor temperature fluctuated by 4.1 °C (from 4.5 °C to 8.6 °C) in the NKCD and 7.3 °C (from 5.2 °C to 12.6 °C) in the KCD. Compared with the large fluctuation in the outdoor air temperature, the indoor air temperature in the cave rooms was relatively stable. In addition, the indoor temperature in the KCD was higher than that in the NKCD during the monitoring period, in which the temperature differences were large in the middle period (24–26 January) and then decreased in the later period (27–28 January). Due to the Kang heating, the indoor air temperature of the cave dwelling was increased by an average of 3.1 °C.

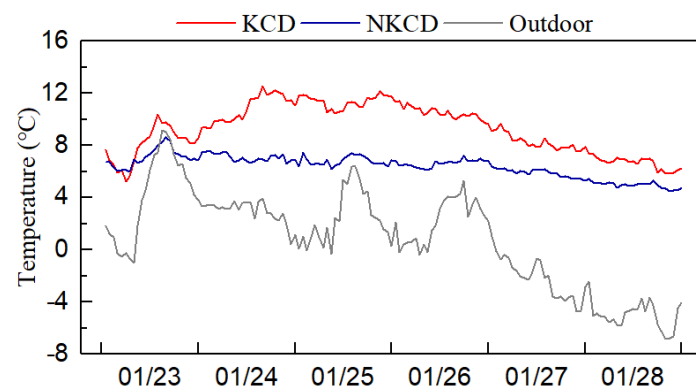


Figure 12. Variation of air temperature.

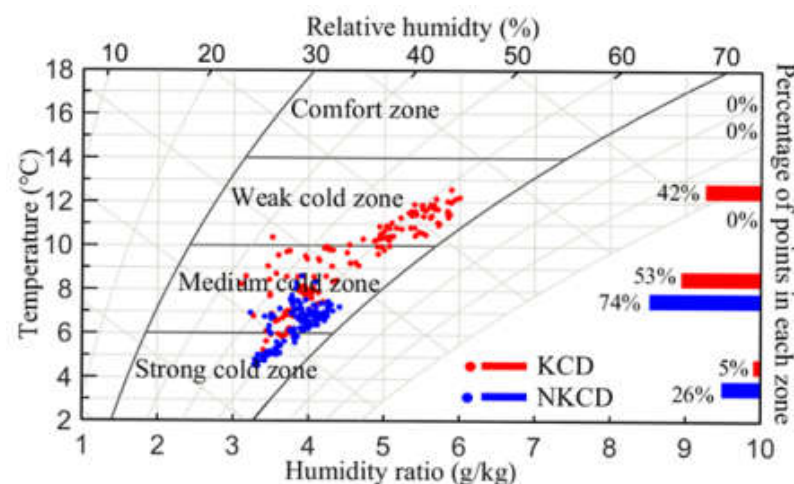


Figure 13. Distribution of air-state points in a psychrometric chart.

The heated indoor temperature was calculated to be 14 °C with a favorable relative humidity between 30% and 70%, according to the Design Standard for Energy Efficiency of Rural Residential Buildings. In a psychrometric chart, this relative humidity range was divided into four sections: comfort zone ( $t \geq 14$  °C), weak cold zone ( $14$  °C  $> t \geq 10$  °C), medium cold zone ( $10$  °C  $> t \geq 6$  °C), and strong cold zone ( $6$  °C  $> t$ ). As shown in Figure 13, the air-state measurement points in the NKCD and KCD did not reach the comfort zone. However, with the heat provided by the Kang, the thermal environment of the cave rooms improved and 42% of the entire monitoring period in the KCD maintained a temperature within the weak cold zone, whereas only 0.05% of the period saw temperatures in the strong cold zone. In contrast, in the NKCD, the air-state measurement points did not even reach the weak cold zone and 26% of the monitoring period remained in the strong cold zone.

### 3.1.2. Spatial Distribution of Indoor Air Temperature

Due to the ample space in the cave rooms, there was a temperature difference within the cave rooms. Here, the spatial distribution of the indoor air temperature along the depth and height of the rooms was analyzed. The distribution of the indoor air temperature within the room according to the daily average value obtained from the monitored data is shown in Figure 14.

Figure 14a shows that the indoor air temperature distribution in the NKCD is relatively uniform along with the depth of the room, with a temperature difference between the point furthest from the door and the point nearest to the door ranging between 0.1 °C and 0.5 °C. However, the indoor air temperature in the KCD increased obviously and had a maximum temperature difference of 1.4 °C. The heat accumulation due to the Kang burning resulted in the large temperature difference within the room.

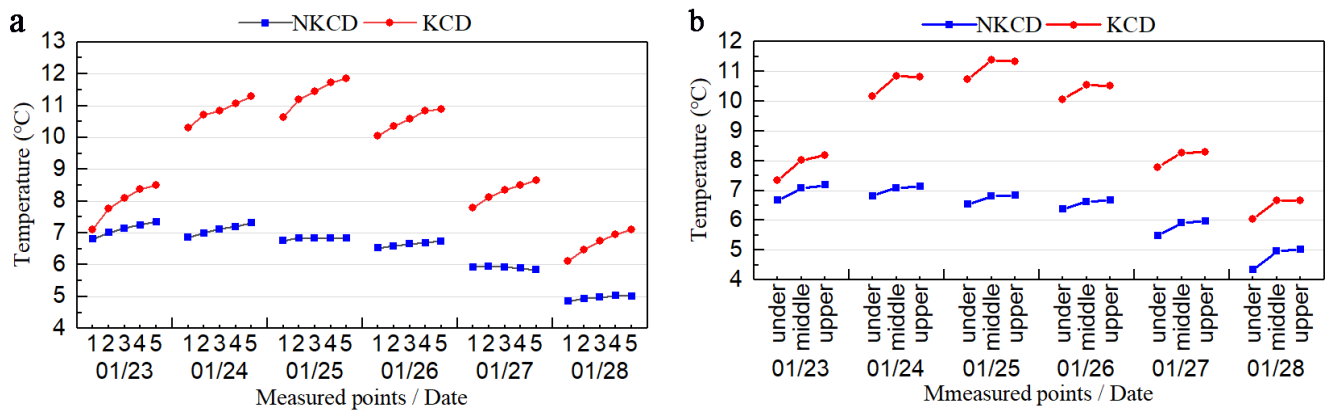


**Figure 14.** Statistics of indoor air temperature distribution along with the depth and height: (a) depth direction; (b) height direction.

Figure 14b shows that the indoor temperature increases with the increase in height within the room. The rate of increase in the temperature per meter of height at the bottom space of the room (the area between the heights of 0.6 m and 1.1 m) in the cave rooms was relatively high. This rate in the NKCD ranged between 0.5 °C/m and 1.3 °C/m, whereas it ranged between 1.0 °C/m and 1.4 °C/m in the KCD. Comparatively, the rate of increase in the temperature per meter of height at the middle of the room (the area between the heights of 1.1 m and 1.7 m) was relatively low, ranging between 0.1 °C/m and 0.2 °C/m in the NKCD and −0.1 °C/m and 0.3 °C/m in the KCD. During four days of monitoring the KCD, there was a drop in temperature along with the height of the room, indicating that the rate of increase in the temperature per meter of height was higher at the bottom region of the cave rooms than at the middle region. According to the statistical data, the air temperature was on average 0.9 °C higher than the surface temperature of the walls at the height of 1.7 m, whereas at the height of 0.6 m, the temperature was only 0.1 °C higher than the surface temperature in the KCD. In the NKCD, this temperature difference at 1.7 m was 1.3 °C and 0.9 °C at 0.6 m.

### 3.2. Thermal Storage Performance of the Heavy Wall

#### 3.2.1. Heat Flux of the Wall

To study the effect of the heavy wall heat charging/discharging on the indoor environment, the heat flux values of the inner wall surface of the NKCD and KCD were obtained, as shown in Figure 15.

From Figure 15a, it can be seen that, whether there was Kang heating or not, the heat flux of the east wall connected to the outside was positive, and the average values were 21.57 W/m<sup>2</sup> (NKCD) and 17.61 W/m<sup>2</sup> (KCD), respectively. Kang heating has a great influence on the heat flux of the inner surface of the west wall. Except for the positive value of the first day, the rest were all negative values, and the average values were respectively 3.48 W/m<sup>2</sup> (NKCD) and −5.89 W/m<sup>2</sup> (KCD) (Figure 15b). When there was no Kang heating, the heat flux of the inner surface of the two side walls was positive, indicating the heat loss from the room. However, when the Kang was burning, the heat flux of the inner surface to the south wall was negative in the later period and heat was released to the room. The average value was −0.31 W/m<sup>2</sup>, while that of the north wall was still positive. Comparing the heat flux of the inner surface of the four walls, it can be seen that, because the east outer wall was connected to the outdoor environment, it was the main wall of indoor heat loss, while the west inner wall far away from the outdoor environment became the main wall for heating when the Kang was burning.

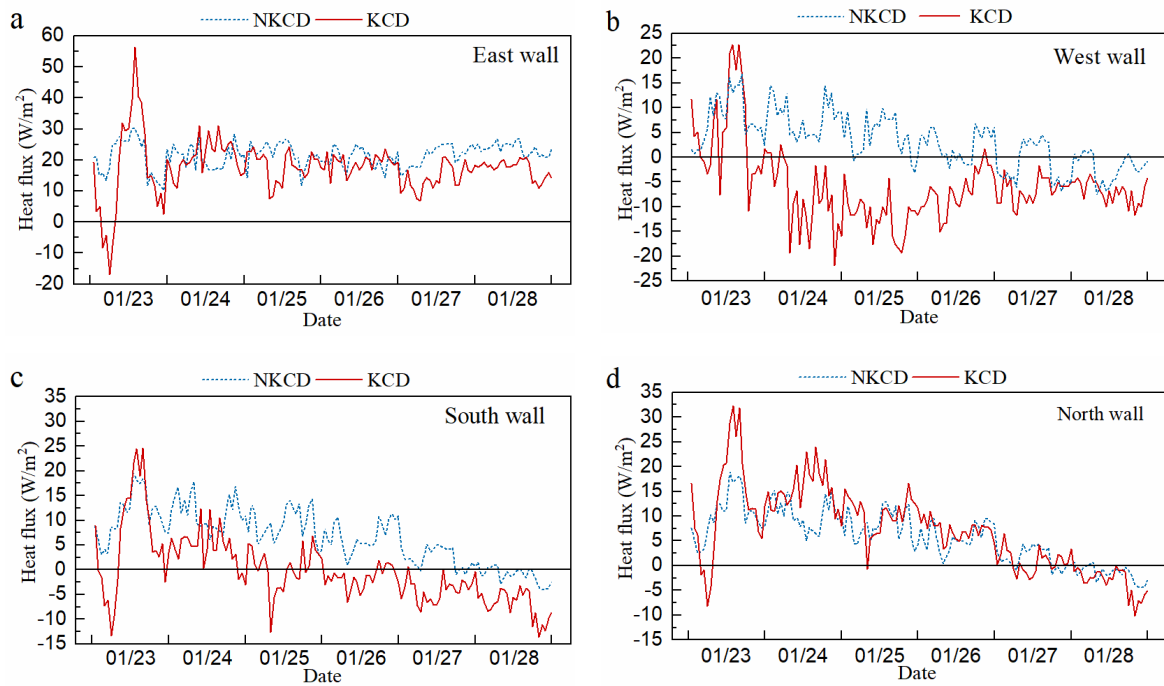


**Figure 15.** Heat flux of inner surface: (a) east external wall; (b) west internal wall; (c) south side wall; (d) north side wall.

### 3.2.2. Thermal Storage of the Inner Wall

Statistics were calculated on the heat storage and release of the wall, as shown in Figure 16. As the east external wall is connected with the external environment and not an indoor thermal storage structure, the east external wall was not considered in the calculation of heat storage and release.

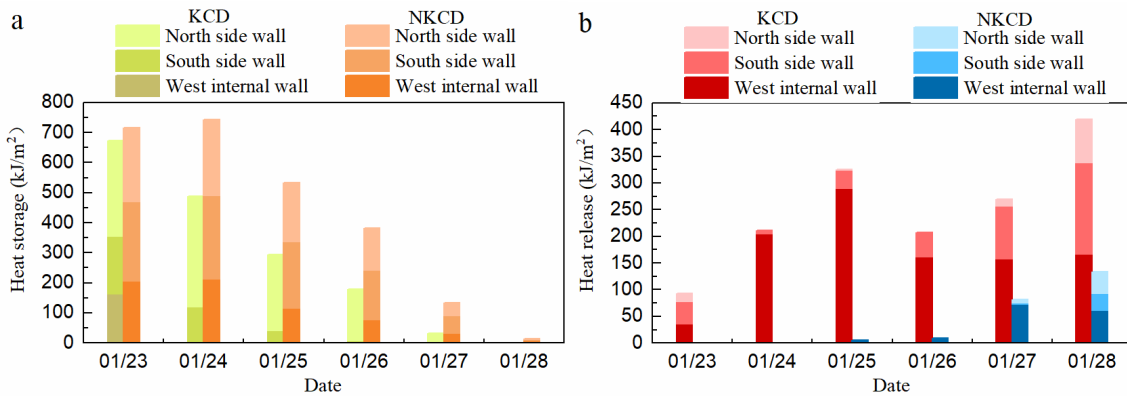


**Figure 16.** (a) Heat storage of the inner wall; (b) heat release of the inner wall.

It can be seen in Figure 16a that, during the test period, the heat storage of the wall showed a gradual decrease trend. The maximum heat storage of KCD appeared on the first day, and the value was 672.59 kJ/(m<sup>2</sup>). The maximum heat storage of NKCD appeared on the second day, and the value was 741.92 kJ/(m<sup>2</sup>). In addition, comparing the heat storage of each wall, it can be found that the largest heat storage in KCD was the north side wall, while the largest heat storage in NKCD was the south side wall, and the heat storage of the north side wall in NKCD was slightly lower than that of the south side wall. As shown in Figure 16b, the wall of KCD released the heat every day during the test period, and the value was between 93.29 kJ/(m<sup>2</sup>) and 419.02 kJ/(m<sup>2</sup>). However, only a small amount of heat was released from the wall of NKCD in the later periods of the test, and the max heat release was 134.03 kJ/(m<sup>2</sup>). Comparing the heat release of the four walls

in the KCD, it can be found that the west inner wall was the main heat release wall, and the heat release was stable, followed by the south side wall, which began to release more heat in the later periods.

The release-storage coefficient  $r$  (ratio of heat release to storage) is introduced to illustrate the thermal storage-release characteristics. As can be seen in Figure 16, the period of heat storage-release was long in the cave rooms; therefore, the whole monitoring period was taken as the unit time. The statistics of the release-charge coefficient  $r$  for each inner wall surface are shown in Figure 17.

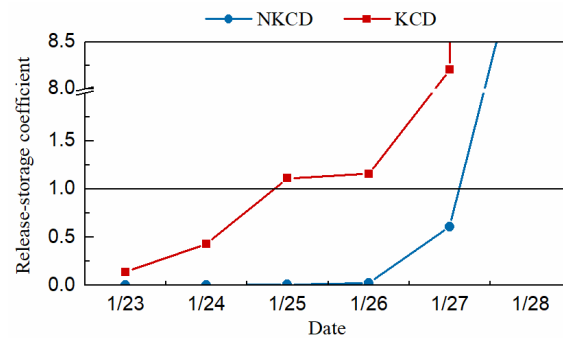


Figure 17. Release-storage coefficient of inner surfaces.

As shown in Figure 17, the release-storage coefficient of the inner wall in KCD rose slowly. On the third day, the release-storage coefficient began to be greater than 1 and then rose rapidly. Relatively, the release-storage coefficient of the inner wall in NKCD was close to 0 in the early period and suddenly rose sharply in the later period. This indicates that the KCD stored heat in the early period and released it to the indoor air slowly when the outdoor temperature dropped in the later period, keeping the indoor temperature stable. In the NKCD, the release-storage coefficient was basically 0 in the early period, indicating that the heat stored in the wall was basically lost by heat conduction into the earth. In addition, because the heat storage of the NKCD in the later period was also small, although the release-storage coefficient was relatively large, the heat release was still less, which was not enough to maintain the indoor air temperature.

### 3.2.3. Heat Release of Walls during the Night

Due to the lack of solar irradiance during the night, the heat release of the wall becomes the only heat source, rendering it essential for maintaining the indoor air temperature. Therefore, the heat release during the night was evaluated, as shown in Figure 18. According to the time of sunrise and sunset in Sanmenxia city, the day period was set as 08:00 to 18:00 and the night period was set as 18:00 to 08:00 the next day.

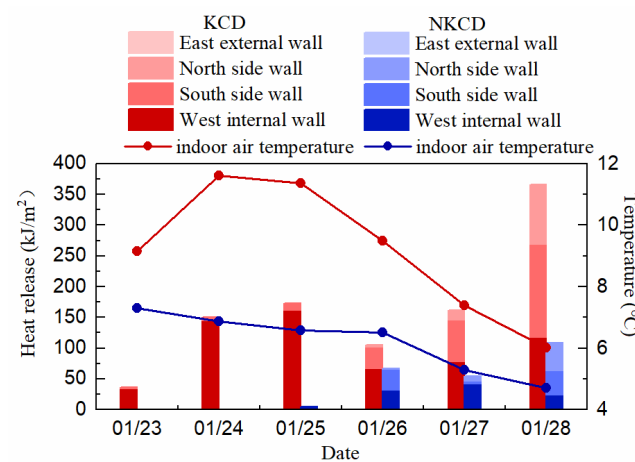


Figure 18. Heat release of walls during the night.

As shown in Figure 18, during the entire monitoring period, heat was released during the night in the KCD, and the total heat released from the inner wall ranged between 36.07 and 366.377 kJ/m<sup>2</sup>, which is greater than that in the NKCD. This indicates that the heat release performance of the KCD at night was better than that of the NKCD. Comparing the heat release of the four walls of the KCD, it can be found that, in the early and middle periods of Kang burning, the west inner wall was the main heat-releasing wall at night. In the later period of Kang burning, however, the heat release of the south and north side walls gradually increased and became the main heat discharging walls. There was no heat release from the east wall at night.

### 3.3. Thermal Performance of the Heavy Wall under Double-Sided Thermal Effect

According to the analysis above, the thermal storage-release characteristic of the external wall was relatively poor compared with the internal wall. However, as the only wall directly connected to the outdoor environment, the external wall plays an important role in dampening the influence of the outdoor environment fluctuations on the indoor thermal environment. Therefore, monitoring data for 23 January were selected for analysis and based on the harmonic response method and established the analytical solution of unsteady heat transfer of the external wall under double-sided thermal effect.

#### 3.3.1. Thermal Frequency Response of the External Wall

Because the indoor and outdoor thermal effects were expanded to six orders, the attenuation multiple and delay time of the first six orders of the temperature were calculated.

As shown in Table 5, for the first-order harmonic, the delay time in the thermal frequency response of heat transfer of the external wall was 12.22 h, and with the increase in order, the attenuation multiple of the heat transfer increased exponentially, and the delay time decreased rapidly. In contrast, the attenuation multiple of the endotherm increased slowly, and the delay time decreased slowly.

**Table 5.** Thermal frequency response of the external wall of selected underground cave-dwelling.

Orders	Thermal Frequency Response of Heat Transfer			Thermal Frequency Response of Endothermic		
	Attenuation Multiple	Delay Time (h)	Delay Phase (rad)	Attenuation Multiple	Delay Time (h)	Delay Phase (rad)
1	42.28	12.22	3.20	1.27	0.44	0.12
2	158.86	8.71	4.56	1.32	0.31	0.16
3	438.96	7.14	5.61	1.37	0.26	0.21
4	1037.00	0.21	0.22	1.42	0.23	0.24
5	2220.40	0.77	1.00	1.47	0.21	0.27
6	4434.50	1.09	1.71	1.52	0.19	0.30

#### 3.3.2. Composition of Unsteady Heat Transfer of the External Wall

According to Equations (11)–(14), the steady heat transfer ( $q_s$ ) and the additional heat transfer ( $q_r$  and  $q_a$ ) caused by the fluctuations in the double-sided thermal effect of the external wall of the KCD can be obtained, as shown in Figure 19. Here, the heat transfer components and superposition process of the external wall are displayed, in which the positive value implies that heat flows out from the inside to the outside and the negative value implies that heat flows inside from the outside.

Figure 19 shows that with the use of Kang heating, the unsteady heat transfer of the external wall can be considered as the superposition of the additional heat transfer ( $q_a$ ) caused by outdoor thermal effect, the steady heat transfer ( $q_s$ ), and the additional heat transfer ( $q_r$ ) caused by internal effects. The heat flux is integrated to obtain the heat transfer of the external wall. It was observed that the external wall was always in a state of exuding heat to the outside throughout the day. However, there were fluctuations in the external wall heat transfer that averaged 9.13 W/m<sup>2</sup> with an amplitude of 6.07 W/m<sup>2</sup>. The maximum heat transfer flux appeared at 14:00 and the minimum appeared at 4:00. The majority of the heat loss occurred in the daytime, accounting for 66.24% of the total heat

loss. Although the outdoor environment temperature decreased at night, the cave room did not lose much heat. The indoor air temperature maintained a small fluctuation throughout the day.

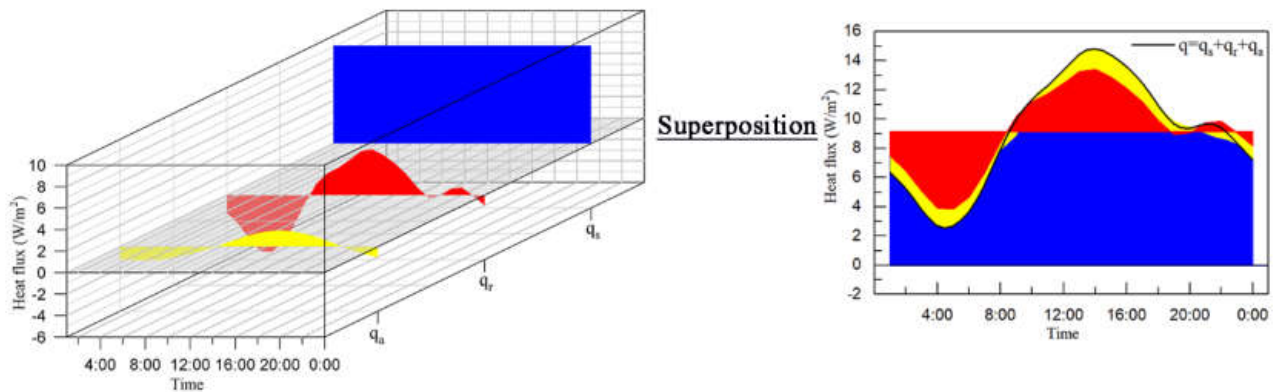


**Figure 19.** Heat transfer components and superposition of the external wall.

### 3.3.3. Thermal Storage Performance of the External Wall

Although the exterior wall is relatively poor compared with the inner wall, it still has a large heat storage capacity. Therefore, we compared the heat flux on the interior surface and heat loss of the external wall of KCD (Figure 20).

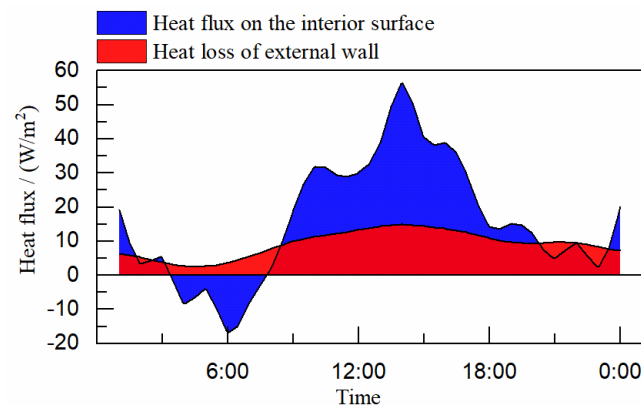


**Figure 20.** Heat flux on the interior surface and heat loss of external wall.

As shown in Figure 20, it can be found that the fluctuation behaviors of heat flux on the interior surface and heat loss of the external wall are similar. However, the amplitude of the heat flux on the interior surface was  $36.54 \text{ W/m}^2$ , which is much larger than the amplitude of the heat loss of the external wall, which was  $6.07 \text{ W/m}^2$ . According to Equations (12)–(15), this phenomenon is caused by the characteristic that the heat transfer attenuation of the heavy wall is much larger than the heat absorption attenuation. Integrating the two curves shows that the difference between the heat storage and the release of the inner wall surface is  $1388.02 \text{ kJ/m}^2$ , and the difference between the heat flowing out to the outside through the external wall and the heat flowing into the inside is  $789.01 \text{ kJ/m}^2$ , resulting in a difference between these two values of  $599.01 \text{ kJ/m}^2$ . Considering the favorable heat storage performance of soil materials, it was inferred that this heat was stored in the wall, confirming that soil cave walls have good heat storage performance.

## 4. Conclusions

Kang heating is intermittent, and when combined with the thermal storage performance of the heavy wall, a favorable indoor thermal environment can be obtained. Based on the monitoring data of the thermal environment in the underground cave dwellings, the thermal environment of the cave rooms and the thermal storage performance of wall

was analyzed quantitatively, and the analytical solution of unsteady heat transfer of the external wall under double-sided thermal effect was established and revealed the thermal storage performance of the wall and mechanism of maintaining indoor thermal environment stability.

In the analysis of the thermal performance of the underground cave dwellings, the variation in the indoor air temperature in time and its distribution in space were determined. Due to Kang heating, the indoor air temperature of cave dwellings could be increased by an average of 3.1 °C. However, regardless of whether there was Kang heating or not, the rate of increase in the temperature per meter of height was higher at the bottom region of the cave rooms than at the middle region.

A comparative analysis of the thermal storage performance of the inner wall between the KCD and NKCD demonstrated that inner walls had a large thermal mass with Kang heating, the maximum heat storage in a single day was 487.75 kJ/m<sup>2</sup>, and the maximum heat release in a single day was 419.02 kJ/m<sup>2</sup>. Moreover, the heat release of the walls at night could reach 366.377 kJ/m<sup>2</sup>, and the release-storage coefficient of the wall was increased significantly with Kang burning, rendering the inner wall an important heat storage mass for the cave rooms to provide heat to the room at night. The heat provided by Kang burning could be fully utilized in the cave room.

Based on the harmonic response method and measured data, an unsteady heat transfer model of the envelope was proposed for the first time. The unsteady heat transfer analysis of the cave's heavy wall shows that, considering low outdoor air temperatures, the heat through the external wall continuously flowed out from the inside. However, the delay time of the external wall to outdoor temperature wave was 12.22 h, which made the heat loss through the external wall during the night only 33.76% total, maintaining a stable indoor thermal environment at night. Moreover, in comparison to heat flux on the interior surface with heat loss of external wall, the thermal storage of the outer wall in a day could reach 599.01 kJ/m<sup>2</sup>.

This study analyzed the indoor thermal environment and the wall's thermal storage performance of the underground cave dwelling envelope under Kang intermittent heating. In addition, based on the unsteady heat transfer model established in this paper, the thermophysical characteristics and structure of the earthen wall can be further optimized to improve the thermal comfort of traditional dwellings. Furthermore, as a general calculation model, the model could provide a theoretical reference for the design of the heavy walls of modern buildings as heat storage equipment.

**Author Contributions:** J.Z.: Conceptualization, Methodology, and Data Curation. Y.L.: Formal Analysis and Writing—Original Draft Preparation. R.L.: Visualization and Investigation. B.C.: Supervision. Y.C.: Writing—Review and Editing. J.L.: Writing—Review and Editing. All authors have read and agreed to the published version of the manuscript.

**Funding:** This research was supported by grants from the Science and Technology Department of Henan Province (grant number, 212102310573), National Natural Science Foundation of China (grant number, 52108100), and Young talents Enterprise Cooperative Innovation Team Project of Zhengzhou University (grant number, 32320408), China Construction Seventh Bureau Technology Research Project (grant number, CSCEC7b-2015-Z-24).

**Institutional Review Board Statement:** Not applicable.

**Informed Consent Statement:** Not applicable.

**Data Availability Statement:** Not applicable.

**Conflicts of Interest:** The funders had no role in the design of the study; in the collection, analyses, or interpretation of data; in the writing of the manuscript, or in the decision to publish the results.

## Nomenclature

$A$	amplitude, °C
$B$	element in the wall Heat Transfer Matrix
$i$	imaginary unit
$k$	heat transfer coefficient, W/(m <sup>2</sup> /K)
$n$	initial ordinal
$N$	number of discrete points in the period
$q$	heat flux, W/m <sup>2</sup>
$t$	temperature, °C
$T$	cycle
Greek symbols	
$\alpha$	heat transfer coefficient, W/(m <sup>2</sup> /K)
$\zeta$	delay time, h
$\tau$	heat dissipation time, h
$\nu$	attenuation multiple
$\varphi$	initial phase, rad
$\psi$	delay phase, rad
$\omega$	frequency
Subscripts	
$a$	outdoor
$an$	outdoor air temperature wave
$e$	nocturnal radiation
$f$	Fourier series expansion
$Im$	imaginary
$kr$	indoor air in cave dwelling with Kang
$kr,f$	Fourier series expansion of indoor air in cave dwelling with Kang
$n$	order of harmonic
$nr$	indoor air in cave dwelling without Kang
$nr,f$	Fourier series expansion of indoor air in cave dwelling without Kang
$U$	solar radiation
$r$	indoor
$rn$	indoor air temperature wave
$R$	ground reflection
$Res$	real
$s$	steady
$yn$	thermal frequency response of heat transfer
$z$	comprehensive
$z,f$	Fourier series expansion of comprehensive
$zn$	thermal frequency response of endothermic

## References

- Parracha, J.L.; Lima, J.; Freire, M.T.; Ferreira, M.; Faria, P. Vernacular earthen buildings from Leiria, Portugal—Architectural survey towards their conservation and retrofitting. *J. Build. Eng.* **2021**, *35*, 102115. [\[CrossRef\]](#)
- Soudani, L.; Woloszyn, M.; Fabbri, A.; Morel, J.C.; Grillet, A.C. Energy evaluation of rammed earth walls using long term in-situ measurements. *Sol. Energy* **2017**, *141*, 70–80. [\[CrossRef\]](#)
- Balaguer, L.; Vegas López-Manzanares, F.O.; Mileto, C.; García-Soriano, L. Assessment of the Thermal Behaviour of Rammed Earth Walls in the Summer Period. *Sustainability* **2019**, *11*, 1924. [\[CrossRef\]](#)
- Miño-Rodríguez, I.; Naranjo-Mendoza, C.; Korolija, I. Thermal Assessment of Low-Cost Rural Housing—A Case Study in the Ecuadorian Andes. *Buildings* **2016**, *6*, 36. [\[CrossRef\]](#)
- Losini, A.E.; Grillet, A.C.; Bellotto, M.; Woloszyn, M.; Dotelli, G. Natural additives and biopolymers for raw earth construction stabilization—A review. *Constr. Build. Mater.* **2021**, *304*, 124507. [\[CrossRef\]](#)
- Zhu, X.R.; Liu, J.P.; Yang, L.; Hu, R.R. Energy performance of a new Yaodong dwelling, in the Loess Plateau of China. *Energy Build.* **2014**, *70*, 159–166. [\[CrossRef\]](#)
- Hou, J.Y.; Wang, J. *Chinese Cave*; Henan Science and Technology Press: Zhengzhou, China, 1999. (In Chinese)
- Zhu, J.Y.; Tong, L.P.; Li, R.X.; Yang, J.Z.; Li, H.X. Annual thermal performance analysis of underground cave dwellings based on climate responsive design. *Renew. Energy* **2020**, *145*, 1633–1646. [\[CrossRef\]](#)
- Zhu, J.Y.; Tong, L.P. Experimental study on the thermal performance of underground cave dwellings with coupled Kang. *Renew. Energy* **2017**, *108*, 156–168. [\[CrossRef\]](#)

10. Zhao, X.; Nie, P.; Zhu, J.Y.; Tong, L.P.; Liu, Y.F. Evaluation of thermal environments for cliff-side cave dwellings in cold region of China. *Renew. Energy* **2020**, *158*, 154–166. [[CrossRef](#)]
11. Zhu, J.Y.; Xing, C.J.; Li, R.X.; Li, C.; Zhao, X. Experimental and theoretical investigation of thermal performance of Kang heating system in China. *Energy Build.* **2020**, *226*, 110344. [[CrossRef](#)]
12. Liu, J.P.; Wang, L.J.; Yoshino, Y.; Liu, Y.F. The thermal mechanism of warm in winter and cool in summer in China traditional vernacular dwellings. *Build. Environ.* **2011**, *46*, 1709–1715. [[CrossRef](#)]
13. Wang, F.; Liu, Y. Thermal Environment of the Courtyard Style Cave Dwelling in Winter. *Energy Build.* **2002**, *34*, 985–1001. [[CrossRef](#)]
14. Li, X.P.; Cui, Y. Field study on indoor thermal environment of sinking cave in Guanzhong Area in winter. *J. Xi'an Univ. Archit. Technol. (Nat. Sci. Ed.)* **2019**, *51*, 591–596.
15. Ma, X.; Zhang, L.; Zhao, J.Y.; Wang, M.Y.; Cheng, Z. The outdoor pedestrian thermal comfort and behavior in a traditional residential settlement—A case study of the cave dwellings in cold winter of China. *Sol. Energy* **2020**, *220*, 130–143. [[CrossRef](#)]
16. Bruno, A.W.; Gallipoli, D.; Perlot, C.; Kallel, H. Thermal performance of fired and unfired earth bricks walls. *J. Build. Eng.* **2020**, *28*, 101017. [[CrossRef](#)]
17. Laborel-Prénon, A.; Magniont, C.E.; Aubert, J.E. Hygrothermal properties of unfired earth bricks: Effect of barley straw, hemp shiv and corn cob addition. *Energy Build.* **2018**, *178*, 265–278. [[CrossRef](#)]
18. Yu, K.C.; Tan, Y.F.; Zhang, T.T.; Zhang, J.D.; Wang, X.M. The traditional Chinese kang and its improvement: A review. *Energy Build.* **2020**, *218*, 110051. [[CrossRef](#)]
19. Heier, J.; Bales, C.; Martin, V. Combining thermal energy storage with buildings—a review. *Renew. Sustain. Energy Rev.* **2015**, *42*, 1305–1325. [[CrossRef](#)]
20. Yang, M.; Yang, X.D.; Wang, Z.F.; Wang, P.S. Thermal analysis of a new solar kang system. *Energy Build.* **2014**, *75*, 531–537. [[CrossRef](#)]
21. Yang, M.; Yang, X.D.; Wang, P.S.; Shan, M.; Deng, J. A new Chinese solar kang and its dynamic heat transfer model. *Energy Build.* **2013**, *62*, 539–549. [[CrossRef](#)]
22. Li, G.; Bi, X.X.; Feng, G.H.; Chi, L.; Zheng, X.F.; Liu, X.T. Phase change material Chinese Kang: Design and experimental performance study. *Renew. Energy* **2020**, *150*, 821–830. [[CrossRef](#)]
23. Bian, M.L. Numerical simulation research on heat transfer characteristics of a Chinese kang. *Case Stud. Therm. Eng.* **2021**, *25*, 100922. [[CrossRef](#)]
24. Feng, G.H.; Sheng, X.; Xu, X.L. Thermal performance analysis of combined heating of phase change kang and firewall for village room under winter condition. *Procedia Eng.* **2016**, *146*, 541–548. [[CrossRef](#)]
25. Xu, J.M.; Xia, N.; Xing, K. Low energy consumption kang design for villages and towns in northeast cold area. *Low Temp. Archit. Technol.* **2016**, *38*, 1–13. (In Chinese)
26. Rathore, P.K.S.; Shukla, S.K. Potential of macroencapsulated PCM for thermal energy storage in buildings: A comprehensive review. *Constr. Build. Mater.* **2019**, *225*, 723–744. [[CrossRef](#)]
27. Romdhane, S.B.; Amamou, A.; Khalifa, R.B.; Saïd, N.M.; Younsi, Z.; Jemni, A. A review on thermal energy storage using phase change materials in passive building applications. *J. Build. Eng.* **2020**, *32*, 101563. [[CrossRef](#)]
28. Reza, D.; Ayman, M.B.; Seth, B.D. NanoPCM based thermal energy storage system for a residential building. *Energy Convers. Manag.* **2022**, *254*, 115208.
29. Iffa, E.; Hun, D.; Salonvaara, M.; Shrestha, S.; Lapsa, M. Performance evaluation of a dynamic wall integrated with active insulation and thermal energy storage systems. *J. Energy Storage* **2022**, *46*, 103815. [[CrossRef](#)]
30. Eldokaishi, A.O.; Abdelsalam, M.Y.; Kamal, M.M.; Abotaleb, H.A. Modeling of water-PCM solar thermal storage system for domestic hot water application using Artificial neural networks. *Appl. Therm. Eng.* **2022**, *204*, 118009. [[CrossRef](#)]
31. Jundika, C.K.; Luthfi, A.F.H.; Iqbal, T.; Chen, L.J.; Jiang, L.S. Optimization of an innovative hybrid thermal energy storage with phase change material (PCM) wall insulator utilizing Taguchi method. *J. Energy Storage* **2022**, *49*, 104067.
32. Wang, H.; Ci, E.D.; Li, X.Q.; Li, J.Q. The magnesium nitrate hexahydrate with TiO<sub>2</sub> composite phase change material for photo-thermal conversion and storage. *Sol. Energy* **2021**, *230*, 462–469. [[CrossRef](#)]
33. Xu, Y.Q.; Luo, C.; Sang, H.Y.; Lu, B.W.; Wu, F.; Li, X.S.; Zhang, L.Q. Structure and surface insight into a temperature-sensitive CaO-based CO<sub>2</sub> sorbent. *Chem. Eng. J.* **2022**, *435*, 134960. [[CrossRef](#)]
34. Xu, Y.Q.; Lu, B.W.; Luo, C.; Wu, F.; Li, X.S.; Zhang, L.Q. Na<sub>2</sub>CO<sub>3</sub> promoted CaO-based heat carrier for thermochemical energy storage in concentrated solar power plants. *Chem. Eng. J.* **2022**, *435*, 134852. [[CrossRef](#)]
35. Xu, Y.; Zhang, T.; Lu, B.W.; Luo, C.; Wu, F.; Li, X.S.; Zhang, L.Q. Glycine tailored effective CaO-based heat carriers for thermochemical energy storage in concentrated solar power plants. *Energy Convers. Manag.* **2021**, *250*, 114886. [[CrossRef](#)]
36. Xu, Y.Q.; Lu, B.W.; Luo, C.; Chen, J.; Zang, Z.W.; Zhang, L.Q. Sorption enhanced steam reforming of ethanol over Ni-based catalyst coupling with high-performance CaO pellets. *Chem. Eng. J.* **2021**, *406*, 126903. [[CrossRef](#)]
37. Brambilla, A.; Jusselme, T. Preventing Overheating in Offices through Thermal Inertial Properties of Compressed Earth Bricks: A Study on a Real Scale Prototype. *Energy Build.* **2017**, *156*, 281–292. [[CrossRef](#)]
38. Romani, J.; Gracia, A.D.; Cabeza, L.F. Simulation and control of thermally activated building systems (TABS). *Energy Build.* **2016**, *127*, 22–42. [[CrossRef](#)]

39. Rhee, K.N.; Olesen, B.W.; Kim, K.W. Ten questions about radiant heating and cooling systems. *Build. Environ.* **2017**, *112*, 367–381. [[CrossRef](#)]
40. Xiao, Y.M.; Liu, X.C.; Zhang, R.R. Calculation of unsteady heat transfer through the envelope of an underground cavern using Z-transfer coefficient method. *Energy Build.* **2012**, *48*, 190–198. [[CrossRef](#)]
41. Lai, Y.M.; Zhang, X.F.; Yu, W.B.; Zhang, S.J.; Liu, Z.Q.; Xiao, J.Z. Three-dimensional nonlinear analysis for the coupled problem of the heat transfer of the surrounding rock and the heat convection between the air and the surrounding rock in cold-region tunnel. *Tunn. Undergr. Space Technol.* **2005**, *20*, 323–332.
42. Rees, S.W.; Zhou, Z.; Thomas, H.R. Ground heat transfer: A numerical simulation of a full-scale experiment. *Build. Environ.* **2007**, *42*, 1478–1488. [[CrossRef](#)]
43. Chen, M. Thermal Performance of Rammed Earth Wall. Master's Thesis, Xi'an University of Architecture and Technology, Xi'an, China, 2017.
44. *JGJ/T 132-2009*; Standard for Energy Efficiency Test of Residential Buildings. Ministry of Housing and Urban-Rural Development of the People's Republic of China: Beijing, China, 2009.
45. Yan, Q.S.; Zhao, Q.Z. *Building Thermal Process*; China Architecture & Building Press: Beijing, China, 1986.
46. *GB 50176-2016*; Code for Thermal Design of Civil Building. Ministry of Housing and Urban-Rural Development of the People's Republic of China. General Administration of Quality Supervision, Inspection and Quarantine of the People's Republic of China: Beijing, China, 2016.
47. ASHRAE. *ASHRAE Handbook of Fundamentals*; ASHRAE: Atlanta, GA, USA, 2009.